Local Structure of Proton-Conducting Lanthanum Tungstate La 28−x W 4+x O 54+δ : a Combined Density Functional Theory and Pair Distribution Function Study

ARTICLE *in* CHEMISTRY OF MATERIALS · MAY 2013

Impact Factor: 8.35 · DOI: 10.1021/cm401466r

CHEMISTRY OF MATERIALS

Article

pubs.acs.org/cm

Local Structure of Proton-Conducting Lanthanum Tungstate $La_{28-x}W_{4+x}O_{54+\delta}$: a Combined Density Functional Theory and Pair Distribution Function Study

Liv-Elisif Kalland,[†] Anna Magrasó,*[,†] Alessandro Mancini,[‡] Cristina Tealdi,[‡] and Lorenzo Malavasi*[,‡]

[†]Department of Chemistry, University of Oslo, Centre for Materials Science an Nanotechnology, FERMiO, Gaustadaléen 21, NO-0349 Oslo, Norway

[‡]University of Pavia and INSTM Unit of Pavia, Viale Taramelli 16, Pavia, Italy.

Supporting Information

ABSTRACT: Lanthanum tungstate ($La_{28-x}W_{4+x}O_{54+\delta}$) is a good proton conductors and exhibits a complex fluorite-type structure. To gain further understanding of the short-range order in the structure we correlate the optimized configurations obtained by density functional theory (DFT) with the experimental atomic pair distribution function analysis (PDF) of time-of-flight neutron and synchrotron X-ray data, collected at room temperature. The local atomic arrangements cannot be described by means of any *average* symmetric structure. Tungsten forms WO_6 octahedra in alternating directions, La1 is mainly 8-fold coordinated in relatively symmetric cubes, and La2 is coordinated with 6 or 7 oxygens in heavily distorted cubes. Both DFT and PDF confirm that the excess tungsten (x) is incorporated in La2 ($^1/_4$, $^1/_4$, $^1/_4$) sites in the $La_{27}W_5O_{55.5}$ composition. This additional tungsten can be considered as a donor self-dopant in the material and has implications to the conducting properties and the defect structure.

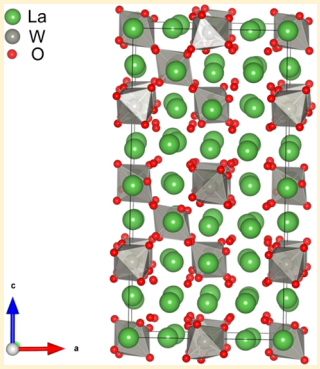

KEYWORDS: *proton conductors, diffraction, pair distribution function analysis, DFT*

INTRODUCTION

Lanthanum tungstate, recently reformulated as $La_{28-x}W_{4+x}O_{54+\delta}v_{2-\delta}$ (where v is the number of oxygen vacancies, and $\delta = 3x/2$),[1] is one of the most interesting ion-conducting materials in the recent times.[1−16] Lanthanum tungstate is a chemically and thermodynamically stable proton and mixed proton−electron conductor which can be used as electrolyte in proton conducting solid oxide fuel cells[10,11] or as a membrane for hydrogen gas separation.[12,13,17] Ionic conductivity in metal oxides is usually enabled by the defects in the structure, and the defects in lanthanum tungstate are present in nominally undoped state, that is, by intrinsic defects.[1] The dopant (intrinsic or extrinsic), the non-stoichiometry, and oxygen vacancies influence the proton concentration *via* the hydration of oxygen vacancies, and are all important defects in high- and intermediate-temperature proton conducting oxides. It is therefore crucial to understand and describe the crystal structure at an atomic level.

The investigation of the crystal structure of lanthanum tungstate has shown to be challenging. The material's stoichiometry was earlier written as La_6WO_{12}, in a similar manner as the smaller rare-earth tungstates (such as Y_6WO_{12} or Ho_6WO_{12}),[18] and no proposals for a full description were presented until recently. In 2009, Magrasó et al.[14] elucidated the first structural model, and determined that the La/W ratio had to be well below 6 for stable phases, more precisely between 5.3 and 5.7 after sintering at 1500 °C. On the basis of neutron and X-ray diffraction, they proposed a fluorite-type cubic structure (space group $F\bar{4}3m$) where the La and W are, on *average*, cubically coordinated by oxygen. In their proposed model, lanthanum occupies 2 different Wyckoff positions, named La1 and La2. La1 sits on *4a* (0, 0, 0) sites, with full occupancy, while La2 sits on *24f* ($^1/_4$, $^1/_4$, $^1/_4$) positions, close to full occupancy. Tungsten is in position *4b* ($^1/_2$, $^1/_2$, $^1/_2$). To account for a lower La/W ratio, the authors proposed two additional positions that were included in the Rietveld refinement. All the oxygen is placed in *16e* sites (x, x, x) with x ~0.13 and x ~0.87.[14]

In 2012, further work established that W is not cubically but octahedrally coordinated at the local scale, based on first principle calculations.[1] Such coordination decreases the maximum number of available oxygen sites from 64 to 56. Consequently, the *stoichiometric* formula is written as $La_{28}W_4O_{54}v_2$. The structural model of this composition is displayed in Figure 1**A**. It was also proposed that the excess W is accommodated in the structure by substitution of lanthanum, and expressed as $La_{28-x}W_{4+x}O_{54+\delta}v_{2-\delta}$. DFT calculations indicated that the WO_6 octahedra adopt alternating directions: La1 as mainly 8-fold coordinated in relatively symmetric cubes, while La2 is coordinated with 6 or 7 oxygens in heavily distorted cubes.[1] These polyhedra are shown in detail in Figure

Received: May 3, 2013
Published: May 7, 2013

   dx.doi.org/10.1021/cm401466r | *Chem. Mater.* 2013, 25, 2378−2384

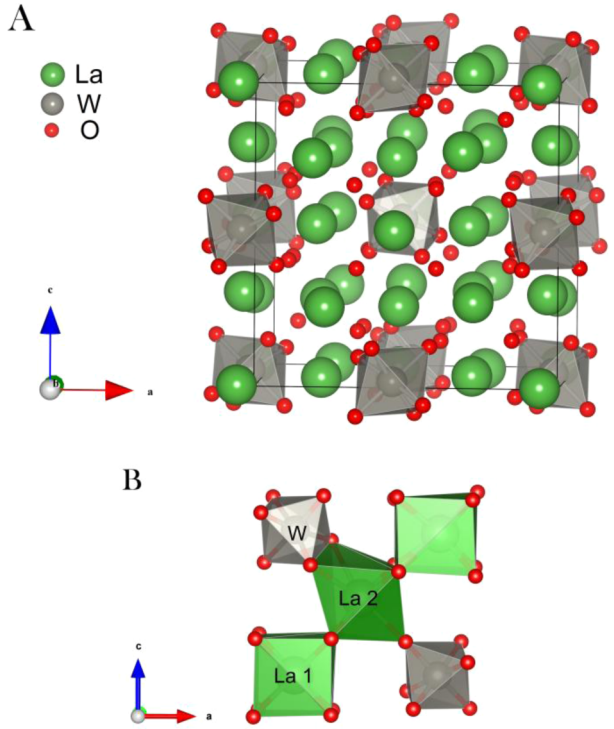

Figure 1. (a) Representative configuration of $La_{28}W_4O_{54}$ relaxed unit cell. It contains 2 vacant oxygen sites. (b) Section of the crystal structure showing the W and La1 and La2 polyhedrons.

1**B**. Small distortions of the cubic structure can only be detected by high resolution X-ray diffraction from a synchrotron source, which were assigned to a tetragonal distortion from the cubic symmetry and refined with the *I*4/*mmm* space group.[1] A summary of the atomic coordinates and lattice parameters for the different studies available in literature are given as Supporting Information.

Neutron diffraction (ND) patterns have shown significant modulation of the background,[14] and the refinement of the ND patterns was found to be more difficult than using X-ray data, both indicative of static disorder in the oxygen sublattice.[1] A recent *in situ* high temperature powder ND study of lanthanum tungstate reports negative mean-square atomic displacements, obtained by the Rietveld method, and supports that the material exhibits localized dynamic disorder of the oxygens around tungsten.[15] Another work using DFT and potential-based calculations have indicated earlier that the complexity of the cell can not be described by the constraints imposed by any space group, especially regarding the oxygen environment around tungsten.[1]

To get further insight into the structural features of lanthanum tungstate and test the available structural models, we will look at the short-range order of this compound by means of the atomic pair distribution function (PDF) analysis of time-of-flight neutron and synchrotron X-ray data, collected at room temperature. After the available reported models are tested, selected configurations from density functional theory (DFT) will be combined with the experimental data from the PDF, and the fine structure of lanthanum tungstate will be investigated in more detail.

The PDF analysis can unveil the short-range order of complex materials, and the strength of the technique is well proven.[19−21] The main advantage is that it takes all the components of the diffraction data (Bragg peaks and diffuse scattering) into account, and thus reveals both the long-range atomic order and the local deviations. DFT is a very powerful and versatile method that uses quantum mechanics for *ab initio* total energy calculations to simulate materials structures and properties. This tool will be used to predict the local atomic arrangements in lanthanum tungstate and test selected models against the experimental data. This will help to clarify the structural characteristics of this complex material.

EXPERIMENTAL SECTION

Powders of lanthanum tungstate with a La/W atomic ratio of 5.4 ($La_{28-x}W_{4+x}O_{54+\delta}$ where x = 1, thereafter referred as LWO54) were prepared by combustion synthesis using EDTA as complexing agent. The reagents were La_2O_3 (99.99% Sigma Aldrich) and WO_3 (99.8% Alfa Aesar), using a procedure described in more detail in ref 15.

Neutron powder diffraction (NPD) measurements at 300 K were carried out on the NPDF diffractometer at the Lujan Center at Los Alamos National Laboratory in a cylindrical vanadium tube. Data from an empty container were also collected to subtract the blank. The corrected total scattering structure function, $S(Q)$, was calculated with the program PDFGETN,[22] and the PDF was obtained by Fourier transformation of $S(Q)$. A Q_{max} = 30.0 Å^{-1} was used. For the X-ray PDF measurements, finely powdered samples were packed in kapton capillaries. X-ray powder diffraction data were collected using a two-dimensional (2D) detector. The experiments were conducted using a synchrotron X-ray diffractometer at the 11-ID-C beamline (wavelength of 0.107980 Å) at the advanced photon source (APS) at Argonne National Laboratory at room temperature. To avoid saturation of the detector, each measurement was carried out in multiple exposures. Each exposure lasted 5 s, and each sample was measured 10 times to improve the counting statistics. The 2D data sets from each sample were combined and integrated using the program FIT2D[23] before further processing. Data from an empty container were also collected to subtract the blank. The corrected total scattering structure function, $S(Q)$, was obtained using standard corrections[19] with the program PDFGETX2.[24] Finally, the PDF was obtained by Fourier transformation of $S(Q)$ according to $G(r) = 2/\pi \int_0^{Q\max} Q[S(Q) - 1]\sin(Qr)\, dQ$ where Q is the magnitude of the scattering vector. A Q_{max} = 28 Å^{-1} was used. Modeling of the experimental neutron and X-ray PDF data was carried out with the aid of PDFGUI and PDFFit2 software.[25]

Preliminary calculations using atomistic techniques by interatomic potentials within the GULP[26] code were used to identify suitable starting configurations. Subsequently the most energetically favorable models were chosen for DFT. The DFT calculations were performed with the VASP code[27−29] with the projector augmented wave (PAW)[30] method. The generalized gradient approximation functional by Perdew, Burke, and Ernzerhof (GGA-PBE)[31] was employed. The unit cell used for the DFT calculations was a 1 × 1 × 2 super cell consisting of two cubic unit cells of $La_{28-x}W_{4+x}O_{54+\delta}v_{2-\delta}$ (where δ = 3x/2 and x = 1, LWO54). DFT calculations do not allow structures containing atoms with partial occupancy, and a double cell was needed to attain an integer number of atoms and vacant sites (*i.e.*, $La_{54}W_{10}O_{111}v_1$). These configurations involve 175 atoms, and one vacant site. Various locations of the vacant oxygen site and different relative directions of the WO_6 octahedra were assayed in the search of low energy configurations (more details are described in the Supporting Information). For the composition without tungsten excess ($La_{28-x}W_{4+x}O_{54+\delta}v_{2-\delta}$, where δ = 3x/2 and x = 0, $La_{28}W_4O_{54}$), no supercell was needed to obtain an integer number of atoms. It is worth mentioning here that tungsten is octahedrally coordinated, and that there are many possible orientations of these octahedra relative to each other. This leads to many possible oxygen sites around tungsten (6 × 4 = 24), but only 6 can be filled simultaneously. These octahedra may flip and change orientation over time, but this may only happen at very high temperatures (typically above 1400 °C or so). This will likely not occur at room temperature, so dynamic disorder will be excluded

dx.doi.org/10.1021/cm401466r | *Chem. Mater.* 2013, 25, 2378−2384

under the conditions we have performed our study (room temperature).

The k-point grid density was set to 1 × 1 × 1 and the wavelength energy cutoff to 400 eV for all calculations. Additional tests using enhanced parameters gave no further improvement to the PDF fit. Relaxation was performed with constant volume with cell parameters from NDP results[14] allowing only the atomic positions to relax. The choice is explained by the observation of some calculated configurations having more than 1% distortion of the cell parameters, when simulated under constant pressure with GULP. Since the calculated configurations are viewed as different possible configurations within a static disordered system, the cell parameters have to be compatible. Also bond distances are usually not affected noticeably for DFT-calculations with constant volume and pressure, and the end cell parameters we obtained, were within the degree of uncertainty.

RESULTS AND DISCUSSION

Figure 2 shows the experimental and fitted X-ray and neutron PDFs of LWO54 (La/W ratio = 5.4, that is, $La_{28-x}W_{4+x}O_{54+\delta}$

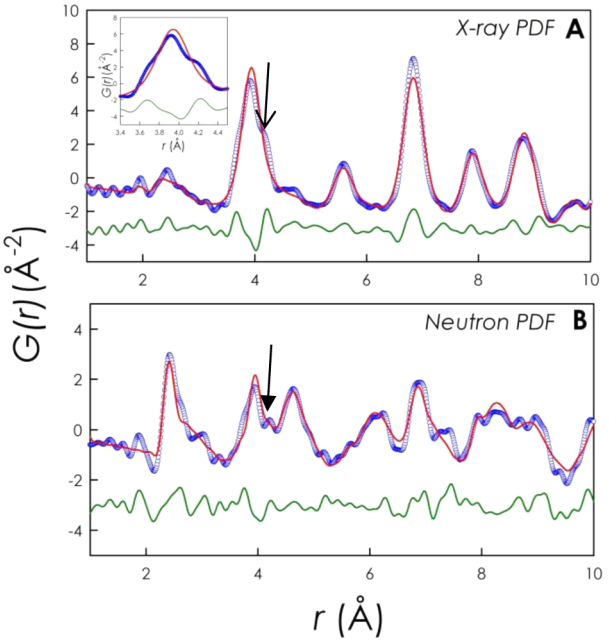

Figure 2. X-ray (Panel A) and neutron (Panel B) PDF refinements of LWO54 by means of the *average* tetragonal space group reported in ref 1. Inset of Panel A: detailed view of a selected region around the peak located at ∼4 Å. Blue circles: experimental data; red line: calculated PDF; and horizontal green line: residual (shifted by −3 for ease of visualization).

with $x = 1$) by means of the tetragonal average model reported in ref 1. (space group $I4/mmm$).

The X-ray PDF fit with the cubic[14] (Supporting Information) and tetragonal[1] structural models (Figure 2**A**, agreement factor: $R_w = 0.188$) describes most of the experimental observed general features of the PDF, with essentially no differences between the two space groups. In these fits, the lattice parameters, atomic positions, and a single atomic displacement parameter for each atom type are refined. It is worth noticing that the first intense peak located at about 4 Å is not symmetric in the experimental data. There are two visible shoulders: a small one at lower *r*-values (with respect to the peak maximum) and a more pronounced shoulder at higher *r*-values. This overall peak mainly contains contributions from all the possible pairs between La, W, and O atoms and all these bond pairs are interpolyhedra connections. The intensity in this case is dominated by the La−La and La−W distances because of the use of the X-ray probe. In the tetragonal (or cubic) symmetry, the local arrangement around W and La atoms sharing the same Wyckoff position is the same, and the model predicts a single symmetric peak. The distribution of intrapolyhedra bond lengths is significantly broader in the real material than the narrow and regular distribution expected from the proposed space group. It is also interesting to note that the shoulder at higher *r*-values on the peak at ∼4 Å in the X-ray PDF corresponds to a separated peak in the neutron PDF (both marked with an arrow in Figure 2). Overall, from the X-ray PDF results, one may conclude that most of the heavy atoms positions in the experimental local structure are not far from those found in the *average* model but that the individual La−La and La−W distances given by this model cannot describe the "real" distortions of the polyhedra.

These considerations are even more evident for the neutron data. The neutron PDF (Figure 2**B**) is poorly described by the structural model from ref 1 ($R_w = 0.327$). The agreement factor and the visual inspection of the fit when using the tetragonal or the cubic models are marginal, an indication that the distortions from cubicity do not explain the low agreement factor. Any attempt to describe the experimental neutron PDF data with maximal subgroups related to the $F\bar{4}3m$ or $I4/mmm$ space groups failed, so a reduction of symmetry does not imply an improvement of the structural model. The main reason is that the contribution from oxygen atoms has a stronger impact on the experimental ND data and, in addition, the disorder and the diffuse scattering observed earlier are now reflected in the PDF. The region at ∼2.4 Å in the neutron PDF (c.f. Figure 2**B**), dominated by intrapolyhedra La−O pairs, is not well described by the model. From the structure of LWO54 calculated by DFT earlier,[1] it is expected that the distribution of La−O pairs is significantly broader than the one calculated from the *average* structure.

At this point, it is clear that a different approach must be taken to find a more detailed description of the local arrangement of the atoms for this material. We have chosen to correlate the experimental PDF data collected for LWO54 with selected configurations calculated by DFT. Since the degree of disorder in the oxygen sublattice is higher than the cation sublattice we will focus on the combination of the DFT and neutron PDF data first, and with X-ray PDF later in the manuscript. When DFT calculated models were used for the refinements, the only parameters refined were the scale factor, lattice parameters, and one atomic displacement parameter (*a.d.p.*) for each group of atoms. The atomic positions were not refined because the cell contains 175 atoms in unique positions.

The first combined DFT-PDF test confirms the presence of the "extra tungsten" (x) on La sites. Figure 3**A** shows the fit of the DFT calculated structure for the $La_{28}W_4O_{54}$ against the experimental neutron PDF for LWO54. It is clear that this model describes poorly the experimental PDF both in terms of peak positions and intensity, although the fit ($R_w = 0.301$) is slightly better than using the *average* model ($R_w = 0.327$). The main peaks with the highest mismatch are those around 2.5 Å (La−O and O−O intrapolyhedra pairs) and the region around ∼3.5 and ∼4.5 Å (interpolyhedra pairs). This deviation will be ascribed (in the coming paragraphs) to the presence of W_{La} and its implications to the structure symmetry and composition, which can obviously not be seen when this defect has not been taken into account.

dx.doi.org/10.1021/cm401466r | *Chem. Mater.* 2013, 25, 2378−2384

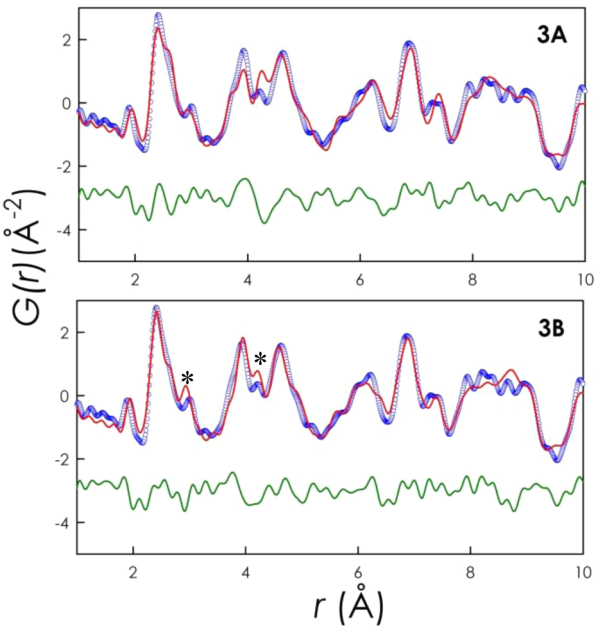

Figure 3. (A) Neutron PDF refinement by means of DFT calculated local structure for the stoichiometric composition (*configuration 0*, Table 1). Blue circles: experimental data; red line: calculated PDF; and horizontal green line: residual (shifted by −3 for ease of visualization); (B) Neutron PDF refinement by means of DFT calculated local structure for the W-excess composition with W on the La1 site (*configuration 1*, Table 1). Blue circles: experimental data; red line: calculated PDF; and horizontal green line: residual (shifted by −3 for ease of visualization).

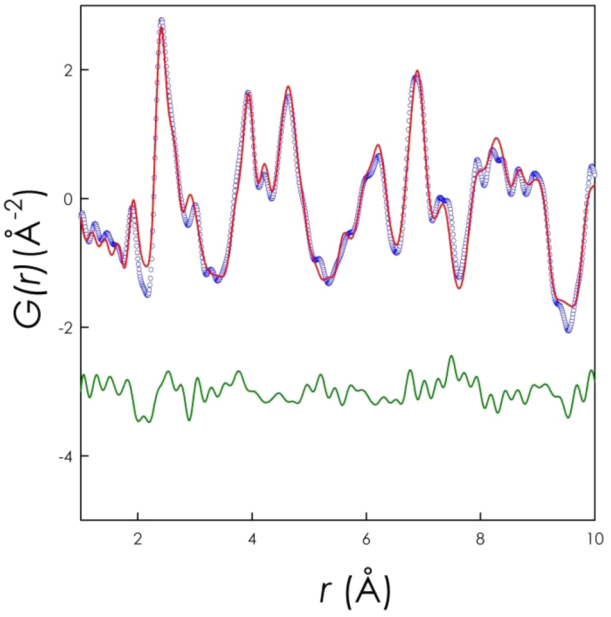

Figure 4. Neutron PDF refinement by means of DFT calculated local structure for the W-excess composition with W on the La2 site (*configuration 5*, Table 1). Blue circles: experimental data; red line: calculated PDF; and horizontal green line: residual (shifted by −3 for ease of visualization).

There are two possible La sites in which to incorporate the W_{La} substitutional defect to form the stable $La_{54}W_{10}O_{111}$ composition: La1 and La2. Table 1 shows that W substitution on La2 is clearly more favorable than on La1. The total energy of the DFT configurations when W sits on La1 sites instead of La2 sites is about 3 to 4 eV higher in energy than the low energy configurations obtained by DFT on the super cell, and the PDF confirms this tendency to be real. The experimental neutron PDF with the DFT calculated model considering W substituting on the La1 site (R_w = 0.286), and on the La2 site (R_w = 0.198) are shown in Figures 3**B** and 4, respectively. La1 is only surrounded by La2 as the nearest neighboring cation, so when W sits on the La1 site, the $W_{La1}O_6$ octahedra are not connected to the regular WO_6 octahedra and the coordination of La2 increases. These results in the appearance of additional intensities that are not found in the experimental data (see the peaks marked with an asterisk in Figure 3**B**). On the other hand, La2 shares oxygen sites with W and La1, and other La2. If W sits on the La2 site, the $W_{La2}O_6$ octahedra are connected to the regular WO_6 octahedra and leads to a lower coordination of La2. Clarifying drawings of this substitution are included as Supporting Information. The reason for such preference is that La2 presents a highly distorted environment (6- and 7- fold coordinated) and is flexible to the substitution by W. La1, on the other side, is surrounded by a quite regular oxygen arrangement with higher coordination number and longer cation-to-oxygen bond length, and will likely not accommodate a small cation such as W(VI).

It is interesting to note that the agreement between the DFT calculated structure (at 0 K) and the experimental PDF (room temperature) is very good considering that no atomic positions were refined. An important conclusion of this study is that the lowest energy configurations found via DFT calculations are very well correlated with the experimental data obtained from X-ray and ND PDF.

The comparison among the fits shown in Figures 3**A**, 3**B**, and 4 can provide further insight on the local environment of the cations in LWO54. The first main peak at ∼2.5 Å suggests that

Table 1. Summary of the Total Energy of Different Representative Configurations of $La_{28}W_4O_{54}$[a] and $La_{54}W_{10}O_{111}$[b] as Calculated by DFT[c] and the Corresponding Fit with the Neutron PDF[d]

	Formula					
	$La_{28}W_4O_{54}$	$La_{54}W_{10}O_{111}$				
configuration number	0	1	2	3	4	5
W sits on	none	La1	La1	La2	La2	La2
total energy relative to configuration 3 (DFT, in eV)		4.29	2.75	0.0	0.67	0.58
E_f (in eV)	−16.05	−14.81	−16.35	−19.10	−18.43	−18.52
R_w (Neutron PDF)	0.301	0.286	0.255	0.207	0.201	0.198

[a]Conf. 0. [b]Conf. 1-5. [c]Referred to the lowest energy configuration. [d]Energy of formation (E_f) is calculated from the total energy with WO_3 and α-La_2O_3 as reference state, and for $La_{28}W_4O_{54}$, two times the energy is reported for comparison. See Experimental Section and Supporting Information for further details.

dx.doi.org/10.1021/cm401466r | *Chem. Mater.* 2013, 25, 2378−2384

the La−O and O−O pairs bond lengths are broadened by the incorporation of W on La2 sites with respect to the *stoichiometric* composition $La_{28}W_4O_{54}$. It is interesting to note that the two peaks around 4 Å can be properly fitted only if W_{La2} is present, which leads to additional W−O and W−La pairs. In the *stoichiometric* model, most of the La−La distances occur in a quite narrow range (around 4.20−4.25 Å). This renders a rather intense peak around that position, and does not explain the wider distribution found experimentally. The presence of W_{La2}, which links two La1 atoms, smears out the nuclear density of the La−La pair and can describe the additional peaks around 4 Å more correctly.

Another pair worth mentioning is the W−O pair, found in the first peak in the neutron PDF (below ca. 2 Å). The W−O pair occurs at ∼1.92 Å for the *stoichiometric* model (Figure 3**A**), while it decreases to 1.86 Å in the model containing W_{La2} and the peak is suitably centered with respect to the experimental data (Figure 4). The substitution of W on La2 sites increases the oxygen content of the cell, which leads to longer La2−O and shorter W−O distances, an indication that tungsten attracts the oxygen more strongly than La2.

Configuration 5 is one of the low energy local structures with W_{La2} computed with DFT, and gives a satisfactory description of the overall shape of the experimental neutron PDF. The graphical sketch of the structure is drawn in Figure 5. We have

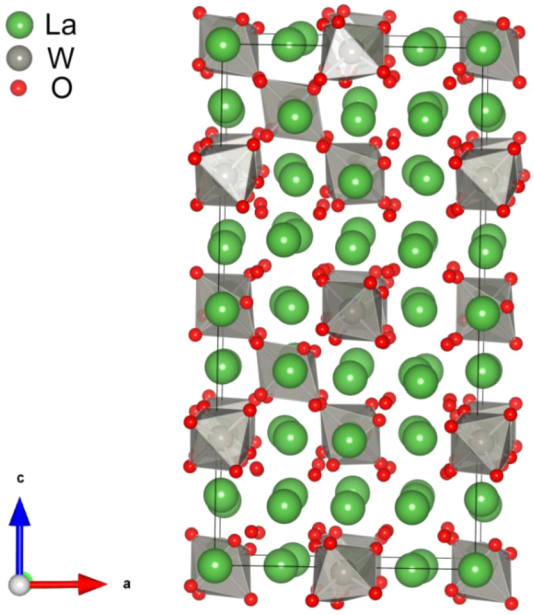

Figure 5. Relaxed unit cell of $La_{54}W_{10}O_{111}$ (2 × 1 × 1 supercell of $La_{27}W_5O_{55.5}$) that corresponds to *configuration 5*. It contains 1 vacant oxygen site and W substituting La on a La2 site.

calculated many other configurations of LWO54 but, for the sake of clarity, only selected examples are shown in Table 1. The main difference between the *configurations 1−5* stems from the various positions of the W_{La} defect (the reader is referred to Supporting Information for a more detailed description). Overall, the models that are >1 eV higher in energy than the most stable configurations (meaning that these are significantly less stable), lead to agreement factors which are higher than 0.2. The configurations with an energy difference <1 eV lead to a good fit (R_w ∼0.2) and are all comparable to *configuration 5*. The energy differences for the different oxygen configurations when W sits on La2 sites are very small (∼ 0.05% energy difference). This most likely means that there are a number of low energy structures involving different connectivity patterns within similar arrangements that are coexisting in the real material. This clearly indicates static disorder in the oxygen lattice as expected from the diffuse scattering in the neutron data.[14] It is also possible that we reach a limit where one cannot distinguish which of the structural models is more representative of the real, measured material, especially when we are measuring such a structurally complex material as in the present case.

All these arrangements result in a switch of the coordination number for some La2 ions (from 7 to 6, and vice versa). This causes small rotations of certain La−O polyhedra and, in some cases, a different direction of the regular WO_6 polyhedra. In general, there is a tendency to obtain relaxed cells with oxygen distributed evenly throughout the cell to reduce the strain. This could explain the reason why the phases with lower La/W ratios are more stable than those with higher lanthanum content: according to $La_{28-x}W_{4+x}O_{54+\delta}v_{2-\delta}$ (where $\delta = 3x/2$), more tungsten leads to a lower concentration of oxygen vacancies, which again results in a higher mean coordination number of lanthanum and, consequently, a more evenly distributed oxygen surrounding La2. It is natural to assume this is more energetically favorable, considering the electrostatic forces at play.

At this point, we consider that the structural model from *configuration 5* can describe the neutron PDF data quite well, and will now be tested against the X-ray PDF data. The fit is shown in Figure 6. It can be appreciated that the fit quality is

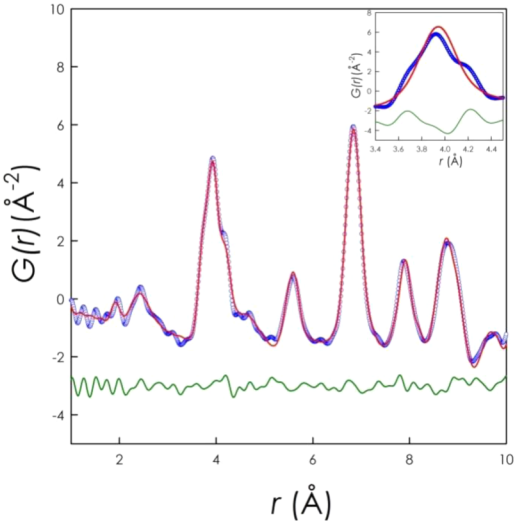

Figure 6. X-ray PDF refinements by means of DFT calculated local structure of low energy, as the one used in Figure 3 for the neutron PDF data. Blue circles: experimental data; red line: calculated PDF; and horizontal green line: residual (shifted by −3 for ease of visualization). Inset: fitted local structure for the tetragonal *average* structure model (same as inset of Figure 2).

very good (R_w = 0.098), and significantly better compared to the first model (R_w = 0.188), cf. Figure 2**A**. A good example is the shape of the intense peak around 4 Å. We mentioned earlier that this peak is dominated by the La−La and La−W contributions (for the X-ray probe). While in the *average* model this is a symmetric peak, the model obtained by DFT calculations can include local structural variations that actually

dx.doi.org/10.1021/cm401466r | *Chem. Mater.* 2013, 25, 2378−2384

occur in the real material. We report that models that do not include W_{La2} lead to a significantly worse fit (R_w = 0.287) compared to the model with W_{La2} (R_w = 0.098). Therefore, both neutron and X-ray PDF confirm the presence of this additional tungsten sitting on La2 sites thus allowing to describe the experimental data in great detail.

As a matter of fact, LWO54 is a good ionic conductor with a degree of disorder in the structure. There are a number of reports in the literature that show similar complex oxides with high ionic conductivity where many low energy configurations were found.[32,33] This has indeed been considered to be a prerequisite for high ionic conductivity since the density of low energy oxygen configurations leads to many low energy transition pathways for ion transport, which enhances ionic conductivity.

It is clear from the data reported here that LWO54 material has a local symmetry which cannot be described by any symmetric structure. The complexity of the structure can not be described accurately within the constraints imposed by a space group's symmetry. The diffuse scattering observed in the ND data, resulting from the static disorder of the oxygen sublattice, makes the investigation of the local structure of this material challenging and must be aided by other techniques. The use of DFT calculations in this case has led to a plausible model to describe the experimental PDF of this complex oxide successfully. The combination of DFT and PDF can provide a very powerful method to understand structural details that may not be sufficiently conclusive from each of the techniques alone.

We have furthermore proved experimentally the presence of tungsten residing in La2 sites, suggested earlier.[1] This means that tungsten acts as a self-donor dopant in lanthanum tungstate. This has direct implications on the materials' properties, such as conductivity and chemical stability, as demonstrated recently by Erdal et al.[16]

CONCLUSION

In this paper we report a combined DFT and PDF investigation of the lanthanum tungstate proton conducting material. We can conclude that the local structure of $La_{27}W_5O_{55.5}$ cannot be described by means of the *average* structure models available in the current literature, particularly for the oxygen environment and a disordered oxygen sublattice. Lanthanum tungstate presents excess tungsten in the structure, which acts as a self-dopant because of intrinsic W_{La} substitutional defects. These defects are located on the La2 site (the substitution is not favorable at the La1 site) due to the higher flexibility of the La2 polyhedra compared to that of La1. Reasonable fits have been obtained for different local structural models considering excess W on the La2 site, thus suggesting that there are a number of low-energy local structures involving different connectivity patterns within the LWO54 structure that may be at the root of the observed high ionic conductivity.

ASSOCIATED CONTENT

Supporting Information

Table of existing structural models for LWO. Table of calculated total energies and formation energies. Description of the selected configurations. Methods for calculating the energy of formation E_f. Buckingham potentials and parameters for the initial calculation with GULP. X-ray PDF fit for LWO54 tested against the Stoichiometric model. This material is available free of charge via the Internet at http://pubs.acs.org.

AUTHOR INFORMATION

Corresponding Author

*E-mail: a.m.sola@smn.uio.no (A.M.), lorenzo.malavasi@unipv.it (L.M.). Fax: +47-22840651 (A.M.), 39 382 987921 (L.M.). Phone: +47-22840660 (A.M.), 39 382 987921 (L.M.).

Notes

The authors declare no competing financial interest.

ACKNOWLEDGMENTS

The authors gratefully acknowledge: the Norwegian metacenter for computational science (Notur) for providing computational resources under the project number NN4604k; financial support from the MIUR through the FIRB project RBFR12CQP5 and the Los Alamos Neutron Science Centre for providing beam time.

REFERENCES

(1) Magraso, A.; Polfus, J. M.; Frontera, C.; Canales-Vazquez, J.; Kalland, L.-E.; Hervoches, C. H.; Erdal, S.; Hancke, R.; Islam, M. S.; Norby, T.; Haugsrud, R. *J. Mater. Chem.* **2012**, *22*, 1762−1764.
(2) Shimura, T.; Fujimoto, S.; Iwahara, H. *Solid State Ionics* **2001**, *143*, 117−123.
(3) Haugsrud, R. *Solid State Ionics* **2007**, *178*, 555−560.
(4) Haugsrud, R.; Kjølseth, C. *J. Phys. Chem. Solids* **2008**, *69*, 1758−1765.
(5) Hancke, R. *Phys. Chem. Chem. Phys.* **2012**, *14*, 13971.
(6) Hancke, R.; Li, Z.; Haugsrud, R. *Int. J. Hydrogen Energy* **2012**, *37*, 8043−8050.
(7) Hancke, R.; Magrasó, A.; Norby, T.; Haugsrud, R. *Solid State Ionics* **2013**, *231*, 25−29.
(8) Lashtabeg, A.; Bradley, J.; Dicks, A.; Auchterlonie, G.; Drennan, J. *J. Solid State Chem.* **2010**, *183*, 1095−1101.
(9) Solis, C.; Escolastico, S.; Haugsrud, R.; Serra, J. M. *J. Phys. Chem. C* **2011**, *115*, 11124−11131.
(10) Solis, C.; Navarrete, L.; Roitsch, S.; Serra, J. M. *J. Mater. Chem.* **2012**, *22*, 16051−16059.
(11) Quarez, E.; Kravchyk, K. V.; Joubert, O. *Solid State Ionics* **2012**, *216*, 19−24.
(12) Escolastico, S.; Solis, C.; Serra, J. M. *Solid State Ionics* **2012**, *216*, 31−35.
(13) Escolastico, S.; Solis, C.; Serra, J. M. *Int. J. Hydrogen Energy* **2011**, *36*, 11946−11954.
(14) Magraso, A.; Frontera, C.; Marrero-Lopez, D.; Nunez, P. *Dalton Trans.* **2009**, 10273−10283.
(15) Magraso, A.; Hervoches, C. H.; Ahmed, I.; Hull, S.; Nordström, J.; Skilbred, A. W. B; Haugsrud, R. *J. Mater. Chem. A* **2013**, *1*, 3774−3782.
(16) Erdal, S.; Kalland, L.-E.; Hancke, R.; Polfus, J.; Haugsrud, R.; Norby, T.; Magraso, A. *Int. J. Hydrogen Energy* **2012**, *37*, 8051−8055.
(17) Erdal, S.; Ph.D. Thesis, University of Oslo, Oslo, Norway, 2011.
(18) Diot, N.; Benard-Rocherulle, P.; Marchand, R. *Powder Diffr.* **2000**, *15*, 220−226.
(19) Egami, T.; Billinge, S. J. L. *Underneath the Bragg Peaks: Structural Analysis of Complex Materials Underneath the Bragg Peaks*; Pergamon: Amsterdam, The Netherlands, 2003.
(20) Malavasi, L.; Kim, H.; Billinge, S. J. L.; Proffen, T.; Tealdi, C.; Flor, G. *J. Am. Chem. Soc.* **2007**, *129*, 6903−6907.
(21) Malavasi, L. *Dalton Trans.* **2011**, *40*, 3777−3788.
(22) Peterson, P. F.; Gutmann, M.; Proffen, T.; Billinge, S. J. L. *J. Appl. Crystallogr.* **2000**, *33*, 1192.
(23) Hammersley, A. P.; Svensson, S. O.; Hanfland, M.; Fitch, A. N.; Hausermann, D. *High Pressure Res.* **1996**, *14*, 235−248.
(24) Qiu, X.; Thompson, J. W.; Billinge, S. J. L. *J. Appl. Crystallogr.* **2004**, *37*, 678.
(25) Farrow, C. L.; Juhas, P.; Liu, J. W.; Bryndin, D.; Bozin, E. S.; Bloch, J.; Proffen, T.; Billinge, S. J. L. *J. Phys.: Condens. Matter* **2007**, *19*, 335219/335211−335219/335217.

(26) Gale, J. D. *J. Chem. Soc., Faraday Trans.* **1997**, *93*, 629−637.
(27) Kresse, G.; Furthmuller, J. *Phys. Rev. B* **1996**, *54*, 11169−11186.
(28) Kresse, G.; Hafner, J. *Phys. Rev. B* **1993**, *48*, 13115−13118.
(29) Kresse, G.; Joubert, D. *Phys. Rev. B* **1999**, *59*, 1758−1775.
(30) Blochl, P. E.; Forst, C. J.; Schimpl, J. *Bull. Mater. Sci.* **2003**, *26*, 33−41.
(31) Perdew, J. P.; Burke, K.; Ernzerhof, M. *Phys. Rev. Lett.* **1996**, *77*, 3865−3868.
(32) Mohn, C. E.; Allan, N. L.; Freeman, C. L.; Ravindran, P.; Stolen, S. *J. Solid State Chem.* **2005**, *178*, 346−355.
(33) Mohn, C. E.; Allan, N. L.; Stolen, S. *Solid State Ionics* **2006**, *177*, 223−228.

■ NOTE ADDED AFTER ASAP PUBLICATION

This article was published ASAP on May 20, 2013, with an error in the Abstract and Table of Contents graphics. The corrected version was published ASAP on May 22, 2013.